Transfer in solids featuring channel flows

2014 EPL 106 64002

(http://iopscience.iop.org/0295-5075/106/6/64002)

A Letters Journal Exploring the Frontiers of Physics

June 2014

EPL, **106** (2014) 64002 www.epljournal.org
doi: 10.1209/0295-5075/106/64002

Transfer in solids featuring channel flows

D. Griffani, P. Rognon and I. Einav

Particles and Grains Laboratory, School of Civil Engineering, The University of Sydney Sydney, NSW 2006, Australia

received on 21 May 2014; accepted by B. Castaing on 6 June 2014
published online 20 June 2014

PACS 44.30.+v – Heat flow in porous media
PACS 91.35.Dc – Heat flow; geothermy
PACS 47.60.Dx – Flows in ducts and channels

Abstract – We investigate the transfer properties of idealised porous materials comprising a diffusive solid pervaded by an array of channels. Using a tracer method, we study how a liquid flowing through these channels may reduce the cooling time of the solid. Accordingly, we define an effective transfer efficiency, which we systematically measure in systems of differing diffusivities, channel radii, lengths and spacings, average flow velocities and flow fields —namely plugged and Hagen-Poiseuille flows. We show that the transfer efficiency scales with a key dimensionless number involving the Péclet number and the channel to solid volume fraction. This scaling exhibits three regimes. Based on the analysis of the advection and diffusion processes in the systems, we introduce a semi-empirical model that captures the entire range of results.

Introduction. – Fractured rocks [1–4] and vascularized tissues [5–9] are examples of porous materials comprising a solid matrix pervaded by a network of channels. The flow of a liquid through these channels may be utilised to transfer heat from or to the surrounding solid. Mammalian thermo-regulation [10], heat extraction from geothermal reservoirs [11–13], and a range of micro-fluidic heat exchangers [14] rely on such a process.

In many applications, the channels are narrow and the flows are slow enough to be laminar. In these cases, the flows within each channel are described by a Hagen-Poiseuille velocity field. Recent works have established how the effective permeability of these types of systems depend on certain network features such as the number of loops [15,16] and the geometry of their branching channels [17,18]. By contrast, when the flowing liquid carries a high concentration of particles like small rock fragments and erythrocytes, the Hagen-Poiseuille velocity field no longer describes the flow. Rather, these suspensions behave as non-Newtonian fluids and tend to produce plugged flows within the channels. The Kozeny-Carman relationship satisfied by systems featuring Hagen-Poiseuille velocity fields [19], can also be used to analyse the effective permeability of those featuring plugged flows [20].

Although flows through channel networks are well understood, quantifying their ability to transfer heat from or to the solid phase is challenging. Studies of systems comprising flows through U-shaped channels, serpentine channels, and tree-shaped channel networks embedded in a conducting solid, have successfully characterised and interpreted their cooling dynamics by measuring a typical cooling time for each system and analysing typical advection and diffusion time scales [12,13,21]. These studies demonstrated the relative improvement in the typical cooling time that may be achieved by introducing greater degrees of system complexity in the form of a greater number of channel bends or generations of branching. However, even for simple channel configurations, there seems to be no general model to predict the typical cooling time as a function of the channel geometry, diffusivity and the nature of the flow.

In this letter, we seek to establish such a model. To this end, we consider an idealised porous material comprising a diffusive solid pervaded by a regular array of advective-diffusive channels. The study is based on systematic cooling numerical experiments performed using a tracer method. We thus investigate the typical cooling time of the solid, and how it depends on key parameters such as the intrinsic diffusivity, channel radius, length and spacing, average flow velocity and flow velocity profile within the channels. We then analyse the fundamental processes of diffusion and advection in such systems to construct a model capable of capturing the measured cooling times over a wide range of these parameters.

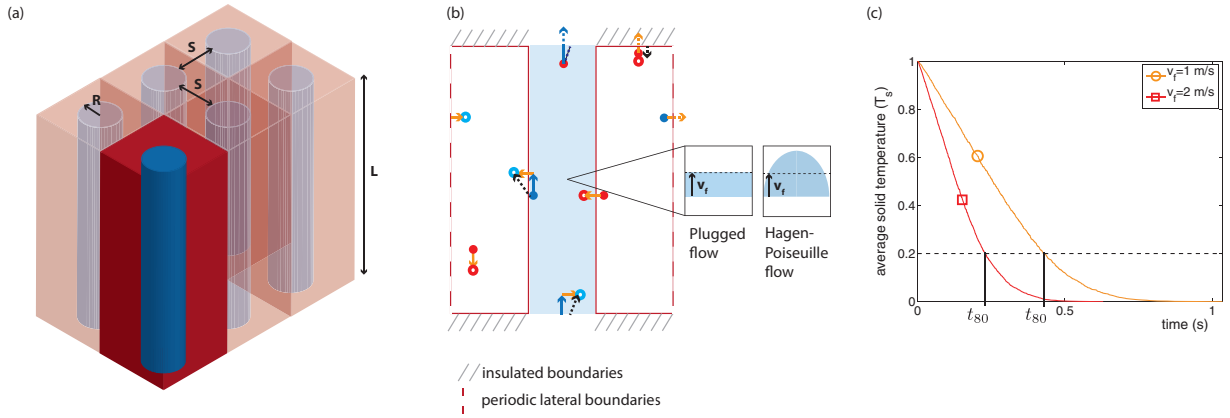

Fig. 1: (Colour on-line) Simulated system. (a) Periodic array of channels of radius R, spacing S and length L embedded in a solid of the same length. Each channel confines a flow of average velocity v_f. (b) Cross-section of a channel and its surrounding solid. The channel may feature either a plugged flow (left inset) or a Hagen-Poiseuille flow (right inset). Typical tracer motions according to the tracer method are illustrated (see text for description). (c) t_{80}: the time required to cool the average temperature of the solid by 80% is identified for two systems. In both systems, $D_0 = 10^{-4}\,\mathrm{m^2/s}$, $R = 0.00125\,\mathrm{m}$, $S = 0.0025\,\mathrm{m}$, $L = 0.1\,\mathrm{m}$, and the channels confine plugged flows, but the average flow velocity (v_f) for one system is double that of the other.

System. – To pin-point the effect of these parameters, we consider idealised systems each comprising a three-dimensional periodic array of equally spaced parallel cylindrical channels embedded in a solid (see fig. 1(a)). Each channel is of radius R and length L, and is encased by a solid of equal length. The spacing between each channel in the array is S. Each channel confines a steady, incompressible flow, characterised by an average flow velocity, v_f and a velocity profile type. We consider two types of velocity profiles, corresponding to plugged and Hagen-Poiseuille flows (see fig. 1(b)). The flowing liquid and the surrounding solid share the same diffusivity, D_0 [$\mathrm{m^2\,s^{-1}}$], specific heat c_p [$\mathrm{J\,K^{-1}\,kg^{-1}}$] and density ρ [$\mathrm{kg\,m^{-3}}$]. Differences between the diffusivity of the liquid and solid phase are not introduced, rather, our investigation focuses on the effects of the selected set of system parameters (R, L, S, v_f, and D_0) across a wide range of values for each flow type.

To deduce the effects of these parameters on the transfer efficiency of a system, we perform *cooling* numerical experiments, where the solid is initially hot and is eventually cooled by the flow of a cold fluid through the channels. The boundary conditions comprise a homogeneous initial temperature in the solid, T_0, insulated boundaries at the top and bottom surface of the solid, and a constant temperature T_{inlet} at the channel inlets (see fig. 1(b)). The local temperature in the system evolves in time according to two modes of transfer: the local diffusion within both the solid and liquid and advection in the liquid. There are no additional exchange terms between the solid and the channel flow. Four typical time scales associated with these modes of transfer (similar to those presented in [12]) can be identified from each system's set of parameters:

$$t_{diff} = \frac{L^2}{D_0}, \quad t_s = \frac{S^2}{D_0}, \quad t_{rad} = \frac{R^2}{D_0}, \quad t_{adv} = \frac{L}{v_f}, \qquad (1)$$

where t_{diff} is the time to diffuse along the length of the solid; t_s is the time to diffuse across the spacing between the channels; t_{rad} is the time to diffuse radially through the fluid in each channel; and t_{adv} is the time for the fluid to travel the length of the channel. Each system can thus be described by three dimensionless numbers:

$$Pe = \frac{t_{diff}}{t_{adv}} = \frac{v_f L}{D_0}, \; \lambda = \sqrt{\frac{t_{diff}}{t_{rad}}} = \frac{L}{R}, \; \gamma = \sqrt{\frac{t_s}{t_{rad}}} = \frac{S}{R}. \qquad (2)$$

The *Péclet number*, Pe, compares the typical diffusion and advection times, λ represents the *slenderness* of each channel, and γ is the *spacing ratio*. Another useful measure, directly related to γ, is the channel to solid *volume fraction*, ϕ, which compares the volume of each channel, Ω_{ch} to the volume of the surrounding solid, Ω_s, as follows:

$$\phi = \frac{\Omega_{ch}}{\Omega_s} = \frac{\pi R^2}{(S+2R)^2 - \pi R^2}. \qquad (3)$$

It can also be expressed as $\phi^{-1} = \frac{1}{\pi}(\gamma+2)^2 - 1$.

Tracer method. – We simulate advection and diffusion in the systems by applying a tracer method similar to those described in [22–24]. In principle, a large number of tracers are initially randomly placed in the system and their motion is integrated over short time steps dt. Their motion includes a random walk component: at each time step, each tracer is assigned a random velocity vector of constant norm $v_0 = \sqrt{\frac{6D_0}{\mathrm{d}t}}$, the orientation of which is selected at random from the six possible orthogonal directions of a cubic lattice [25]. As a result of the random walk, the tracers exhibit a diffusive behaviour described by diffusivity D_0 [22,25]. The advection within each channel is accounted for by superimposing the selected local flow field on the random walk. Typical tracer

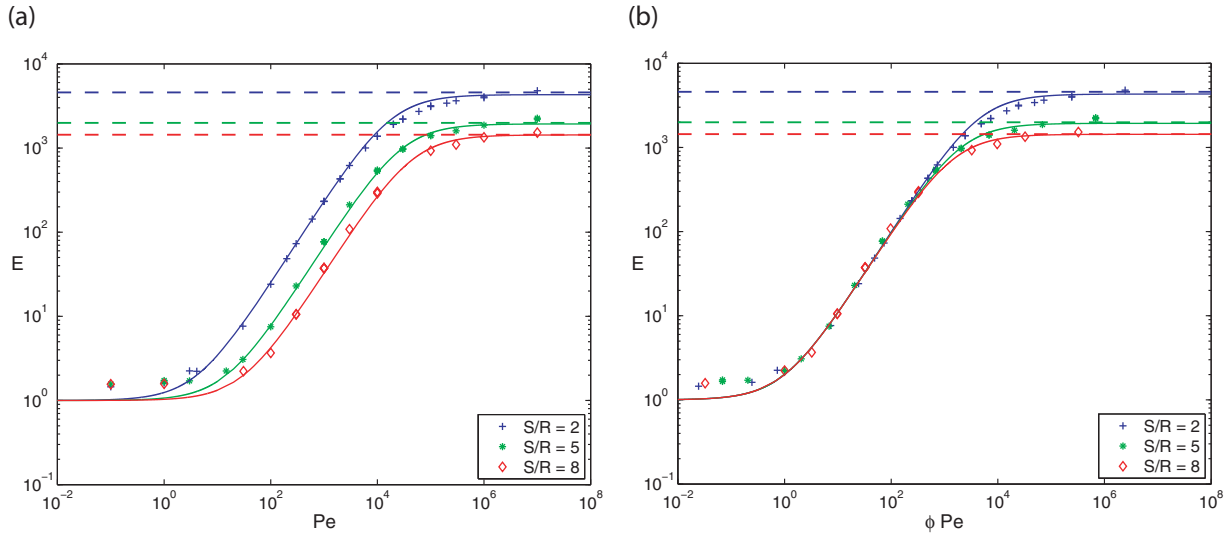

Fig. 2: (Colour on-line) Transfer efficiency results for systems featuring plugged flows. (a) Transfer efficiency as a function of the Péclet number, $Pe = \frac{v_f L}{D}$; (b) transfer efficiency *vs.* the product of the channel to solid volume fraction, ϕ and the Péclet number. In both (a) and (b), the markers denote the simulation results for three different spacing ratios (S/R), and the dashed lines represent the efficiency limits attained for $Pe \to \infty$. The corresponding solid lines represent a plot of the model developed in eq. (10).

motions over one time step are illustrated in fig. 1(b). Random walk (orange arrows) and advection (blue arrows) defines the total displacement (black arrows). The integration scheme comprises an Eulerian first-order integration of the flow of tracers inside the channel followed by the random motion. This scheme is applied to each tracer. The time step adopted for each simulation is the lesser of a fraction of the typical diffusion ($10^{-4}\, t_{rad}$) and advection time ($10^{-4}\, t_{adv}$). The tracer density is fixed at 2×10^9 [tracers/m^3]. We systematically checked that smaller time steps and/or more tracers yield the same results.

Figure 1(b) also illustrates how the system boundary conditions are implemented in the tracer method. Initially, all tracers carry a scalar temperature indicator of magnitude T_0 (red). Tracers exiting the channel outlet are reintroduced at the inlet with a scalar quantity of T_{inlet} (blue). Insulated boundaries are achieved by reflecting back tracers attempting to cross them. Tracers that pass through a periodic lateral boundary, reappear at the opposite boundary. The temperature in a domain of interest can be estimated by averaging the scalar quantities of all the tracers it contains. For instance, the average temperature of the entire solid, $T_s(t)$, is measured at a given point in time, t, by averaging the scalar quantities of all the tracers in the solid at that time.

Measuring the transfer efficiency. – Figure 1(c) presents the evolution of the average temperature in the solid, T_s, of two systems during two cooling experiments. The two systems feature the same properties ($R = 0.00125\,$m, $L = 0.1\,$m, $S = 0.0025\,$m, $D_0 = 10^{-4}\,$m^2/s), with the exception of the average flow velocity of their plugged flows ($v_f = 1\,$m/s compared to $v_f = 2\,$m/s). Cooling is quicker with the faster flow. A typical cooling time, t_x, is defined that corresponds to the time needed for the solid to cool by x per cent such that $T_s(t = t_x) = x\%(T_0 - T_{inlet})$. We adopt $x = 80\%$. This cooling time is then compared to the typical diffusion time, t_{diff}, to define a dimensionless transfer efficiency:

$$E = \frac{t_{diff}}{t_{80}}. \tag{4}$$

Note that the choice of t_{80} as a typical cooling time is arbitrary, and other values could equally be used. We checked that using t_{40}, t_{50} or t_{60} instead of t_{80} did not significantly change the nature of the results presented below.

We first consider systems featuring a plugged flow field within each channel with constant flow velocity, v_f. A set of cooling experiments was conducted varying the average flow velocity, v_f, from 10^{-4} to 10 m/s; the channel (and solid) length, L from 0.1 to 1 m; the channel radius, R from 0.0005 to 0.0125 m; the channel spacing, S from 0.001 to 0.1 m; and the intrinsic diffusivity, D_0 from 10^{-8} to $10^{-4}\,$m^2/s. Figure 2(a) shows the corresponding transfer efficiency as a function of the system's Péclet number, grouping the tests by spacing ratio. Depending on these two dimensionless numbers, a wide range of transfer efficiency values may be achieved, following a seemingly generic family of curves. When re-plotted against the product of the volume fraction, ϕ and the Péclet number in fig. 2(b), the data appear to collapse onto a single curve for low to intermediate values of ϕPe. For relatively larger ϕPe values, the efficiency results appear to approach an asymptotic limit that differs for each spacing ratio tested.

To assess this efficiency limit for each spacing ratio when $Pe \longrightarrow \infty$, we ran a further set of simulations where the flow velocity was set to infinity by forcing all tracers that enter the channel to immediately exit via the channel outlet. The results are presented in fig. 2 as dashed lines. They confirm the existence of a maximum efficiency for $Pe \longrightarrow \infty$, that depends on the spacing ratio.

Modeling the transfer efficiency. – The results in fig. 2 demonstrate a consistent scaling of the transfer efficiency with the Péclet number and the volume fraction. Let us now seek to rationalize these results by developing a minimal model based on the typical rates of diffusion and advection. Tracers typically diffuse along the length of the solid at a rate given by $\frac{1}{t_{diff}}$. When a flow is introduced within the channels, the rate at which tracers are typically advected the length of a channel is $\frac{1}{t_{adv}}$. The model will involve three regimes, summarised in fig. 3.

In a *diffusion-dominant regime*, diffusion can sweep the entire solid volume, Ω_s before the flow is able to flush the volume of the channel, Ω_{ch}. This regime is thus delineated by the condition, $\Omega_s \times \frac{1}{t_{diff}} \geq \Omega_{ch} \times \frac{1}{t_{adv}}$, which can also be expressed as

$$\phi Pe \leq 1. \tag{5}$$

In this diffusion-dominant regime, the flow does not significantly enhance the efficiency of the transfers, leading to an efficiency of the order of 1.

Following the same reasoning, when $\phi Pe > 1$, the flow should enhance the transfer efficiency of the system. This efficiency can be estimated by considering the heat budget of the volume of the solid. This budget includes the evolution of the heat in the solid, $\rho\, c_p\, \Omega_s \dot{T}_s$ and the divergence of the heat flux within the channel, $\rho\, c_p\, \Omega_{ch} v_f \nabla T_{ch}$ where ∇T_{ch} is the average gradient of temperature within the channel. The heat budget can thus be expressed as

$$\dot{T}_s = -\phi v_f \nabla T_{ch}. \tag{6}$$

To deduce the temperature evolution of the solid from this heat budget, the main challenge is to estimate ∇T_{ch}. This can be done by analysing the extent to which the channel is utilised to transport heat from the solid to the outlet. This in turn is linked to the rate at which tracers diffuse from the solid-channel boundary through to the core of the channel given by $\frac{1}{t_{rad}}$.

In the *linear regime*, defined by $\Omega_{ch} \times \frac{1}{t_{rad}} > \Omega_{ch} \times \frac{1}{t_{adv}}$, the entire cross-section of the channel is utilised, as tracers are typically able to carry heat from the solid to the core of the channel before they are flushed to the outlet by the flow. As a result, along the length of the channel, the average temperature within the channel, $T_{ch}(z)$, is assumed to reach the average temperature of the surrounding solid, $T_s(z)$. This assumption is supported by the observed temperature profiles in fig. 4. Accordingly, in this regime, the gradient of temperature in the channel ∇T_{ch} can be approximated by $\frac{T_s - T_{inlet}}{L}$. The heat budget (6) can then be integrated, $\int_{t=0}^{t=t_{80}} -\frac{\mathrm{d}T_s}{T_{inlet}-T_s} = \int_{t=0}^{t=t_{80}} \phi \frac{v_f}{L} \mathrm{d}t$, to determine $t_{80} = -\ln(0.2)\frac{L}{\phi v_f}$. Therefore, the corresponding efficiency scales like

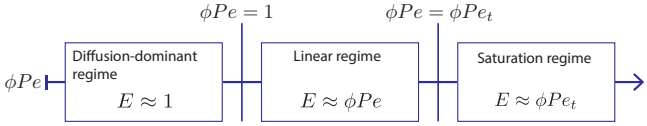

Fig. 3: (Colour on-line) Three regimes of transfer efficiency defined by limiting values of ϕPe.

$$E \approx \phi Pe. \tag{7}$$

We expect this linear regime to end where $\Omega_{ch} \times \frac{1}{t_{rad}} = \Omega_{ch} \times \frac{1}{t_{adv}}$, which corresponds to the Péclet number

$$Pe_t = \frac{L^2}{R^2} = \lambda^2. \tag{8}$$

We enter the *saturation regime* when the Péclet number exceeds this transition value. As the rate at which tracers are flushed along the length of the channel increases relative to the rate at which tracers can diffuse radially, such that $\Omega_{ch} \times \frac{1}{t_{adv}} > \Omega_{ch} \times \frac{1}{t_{rad}}$, a decreasing fraction of the channel's cross-sectional area is utilised to transport heat from the solid to the outlet. As a result, only a relatively small ring-like cross-sectional area close to the channel wall approaches the average temperature of the surrounding solid. The remaining channel core remains at temperatures similar to the cooler fluid inlet temperature, as illustrated in fig. 4. In order for tracers to have the opportunity to diffuse to the core of the channel before reaching the outlet, the channel would need to be longer than L. Specifically, the channel would need to typically be of length $l = v_f t_{rad}$. If this were the case, over the length l, we would expect the average temperature throughout the channel to reach the average temperature of the surrounding solid. Accordingly, the gradient of temperature in the channel in the saturation regime, ∇T_{ch}, can be estimated by $\frac{T_s - T_{inlet}}{l} = \frac{(T_s - T_{inlet})D_0}{v_f R^2}$. Reconsidering the heat budget of the solid from eq. (6) and substituting this estimation of ∇T_{ch} leads to $\int_{t=0}^{t=t_{80}} \frac{\mathrm{d}T_s}{T_s - T_{inlet}} = \int_{t=0}^{t=t_{80}} \phi \frac{D_0}{R^2} \mathrm{d}t$. Solving for t_{80} yields an efficiency in the saturation regime that scales like

$$E = \phi Pe_t. \tag{9}$$

The efficiency in the three identified regimes is summarised in fig. 3 and can be modeled by a single interpolating function. We propose

$$E \approx 1 + \phi Pe \frac{1}{\left(1 + \frac{Pe}{a Pe_t}\right)}, \tag{10}$$

where a is a fitting numerical constant. Figure 2 demonstrates that this function captures all the results across the regimes. Best fits were obtained with values of a ranging from 1 to 1.6.

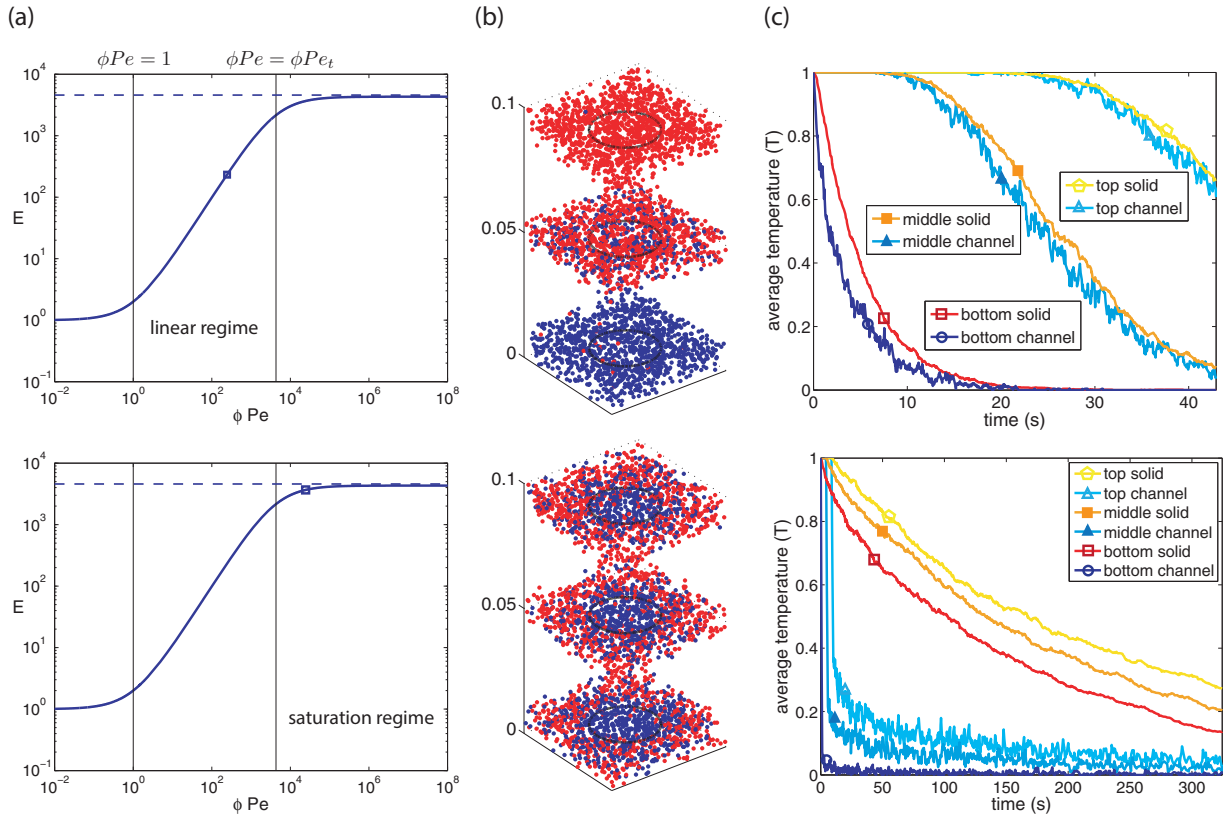

Fig. 4: (Colour on-line) Comparison between two systems where $\frac{S}{R} = 2$ (Top system: $Pe = 10^3$. Bottom system: $Pe = 10^5$). (a) Transfer efficiency as a function of ϕPe from fig. 2. The top system lies in the linear regime. The bottom system falls within the saturation regime. (b) Snapshots of tracers at time t_{40}. Tracers carrying a temperature indicator of T_0 and T_{inlet} are tagged in red and blue, respectively. Three slices each of thickness $\frac{L}{8}$ are pictured: the top slice featuring the channel outlet, the bottom slice featuring the inlet, and a middle slice centered at $\frac{L}{2}$. (c) The temporal evolution of the average temperature within the channel and surrounding solid of each slice. Average temperatures within the channel of the system in the linear regime remain significantly closer to the average temperatures of the surrounding solid as compared to the system in the saturation regime.

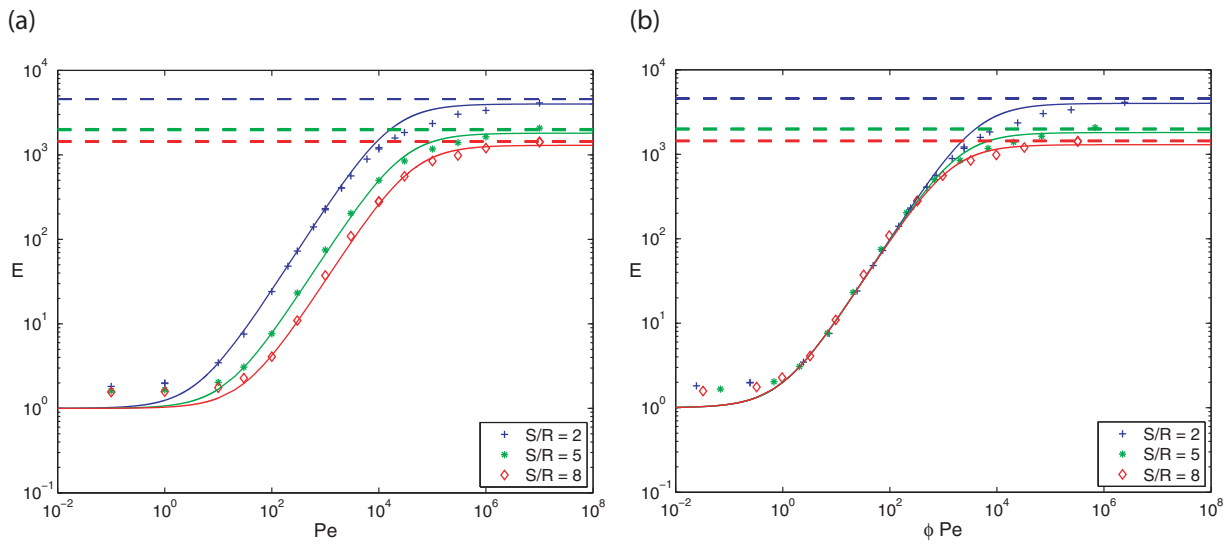

Fig. 5: (Colour on-line) Transfer efficiency results for systems featuring Hagen-Poiseuille flows.

Note that the functional form of the interpolation is not motivated by any physical argument, and other functions could lead to an equally good representation of the results. By contrast, the values of the two transitions and the scaling of the efficiency in the three regimes are well supported by the analysis of the diffusion and advection processes in the system.

Effect of the flow field. – So far, we focused on systems involving a simple velocity profile within the channels, namely the plugged profile. However, in many systems involving laminar flows the flow profiles are not plugged, but rather satisfy the Hagen-Poiseuille equation: $v_i = 2v_f \left(1 - \left(\frac{r}{R}\right)^2\right)$, where r is the radial distance from the centre of the channel.

Given that the flow velocity is maximum in the channel centre, far from the solid, and null at the solid boundary, one could expect such flows to lead to different transfer efficiency results. We have thus repeated the cooling numerical experiments presented in fig. 2, by changing the plugged velocity field to a Hagen-Poiseuille velocity profile with average flow velocity v_f. The corresponding transfer efficiency results are presented in fig. 5. The scaling with ϕPe is very similar to that obtained for plugged flows. It is equally well captured by the semi-empirical model (eq. (10)) with values of a ranging from 1 to 1.6.

Conclusion. – In this study we considered a simple example of porous materials featuring a solid phase pervaded by an array of channels. Analysing such idealised systems proved to be an effective means to pin-point the mechanisms governing the transfers from the solid phase to the liquid flowing though the channels. This analysis, assessed against our numerical results, rationalised the effect of the channel radius, length and spacing, the average flow velocity and flow field, as well as the intrinsic diffusivity on the transfer efficiency of a system. The final outcome is a unique semi-empirical model that captures the transfer efficiency over three regimes; namely, the *diffusion-dominant*, *linear*, and *saturation* regime. These results should constitute a useful framework to further investigate realistic systems involving solids and liquids of differing diffusivities, a wide distribution of channel dimensions and complex networks of channels.

REFERENCES

[1] Greenberg R. J. and Brace W., *J. Geophys. Res.*, **74** (1969) 2099.
[2] Berkowitz B., *Adv. Water Resour.*, **25** (2002) 861.
[3] Bijeljic B., Mostaghimi P. and Blunt M. J., *Phys. Rev. Lett.*, **107** (2011) 204502.
[4] Ronayne M. J., *Adv. Water Resour.*, **56** (2013) 27.
[5] da Fontoura Costa L., Viana M. P. and Beletti M. E., *Appl. Phys. Lett.*, **88** (2006) 033903.
[6] Reichold J., Stampanoni M., Keller A. L., Buck A., Jenny P. and Weber B., *J. Cereb. Blood Flow Metab.*, **29** (2009) 1429.
[7] Barber R. W. and Emerson D. R., *Altern. Lab. Anim.*, **38** (2010) 67.
[8] Miller J. S., Stevens K. R., Yang M. T., Baker B. M., Nguyen D.-H. T., Cohen D. M., Toro E., Chen A. A., Galie P. A., Yu X. *et al.*, *Nat. Mater.*, **11** (2012) 768.
[9] Auger F. A., Gibot L. and Lacroix D., *Annu. Rev. Biomed. Eng.*, **15** (2013) 177.
[10] Li L., Yu B., Liang M., Yang S. and Zou M., *Int. J. Heat Mass Transfer*, **72** (2014) 616.
[11] Ghassemi A., *Geotech. Geol. Eng.*, **30** (2012) 647.
[12] Combelles L., Lorente S., Anderson R. and Bejan A., *J. Appl. Phys.*, **111** (2012) 014902.
[13] Kobayashi H., Lorente S., Anderson R. and Bejan A., *J. Appl. Phys.*, **111** (2012) 044911.
[14] Pence D., *Exp. Therm. Fluid Sci.*, **34** (2010) 474.
[15] Durand M., *Phys. Rev. E*, **73** (2006) 016116.
[16] Durand M., *Phys. Rev. Lett.*, **98** (2007) 088701.
[17] Ronayne M. J. and Gorelick S. M., *Phys. Rev. E*, **73** (2006) 026305.
[18] Kou J., Chen Y., Zhou X., Lu H., Wu F. and Fan J., *Physica A: Stat. Mech. Appl.*, **393** (2014) 527.
[19] Duda A., Koza Z. and Matyka M., *Phys. Rev. E*, **84** (2011) 036319.
[20] Durand M. and Weaire D., *Phys. Rev. E*, **70** (2004) 046125.
[21] Bejan A., Lorente S. and Anderson R., *J. Sol. Energy Eng.*, **136** (2014) 010903.
[22] Griffani D., Rognon P., Metzger B. and Einav I., *Phys. Fluids*, **25** (2013) 093301.
[23] Metzger B., Rahli O. and Yin X., *J. Fluid Mech.*, **724** (2013) 527.
[24] Wang L., Koch D. L., Yin X. and Cohen C., *Phys. Fluids*, **21** (2009) 033303.
[25] Berg H. C., *Random Walks in Biology* (Princeton University Press) 1993.